Correlation Structure of the El Niño/Southern Oscillation Phenomenon

PETER B. WRIGHT* AND JOHN M. WALLACE

Joint Institute for the Study of the Atmosphere and Ocean, University of Washington, AK-40, Seattle, Washington

TODD P. MITCHELL AND CLARA DESER

Department of Atmospheric Sciences, University of Washington, Seattle, Washington

(Manuscript received 13 March 1987, in final form 8 March 1988)

ABSTRACT

Relationships among the atmospheric phenomena associated with the Southern Oscillation and El Niño are investigated, using the Comprehensive Ocean-Atmosphere Data Set (COADS) of marine surface observations from ships of opportunity and the World Monthly Surface [Land] Station Climatology (WMSSC) for the period 1950–79. Annual mean (April–March) sea level pressure at Darwin, Australia is used as an index of the Southern Oscillation. Results are based on simple linear correlation techniques, stratified by season as in the Rasmusson and Carpenter (1982) composite.

Correlations on the order of +0.9 are observed between Darwin pressure, sea surface temperature (SST) and rainfall in the equatorial central Pacific, and zonal wind in the equatorial western Pacific. Relations among these variables are strongest from July through November, when the month to month autocorrelation is also at its strongest. Sea surface temperature along the Peruvian coast and pressure in the eastern Pacific are also most strongly coupled to the Southern Oscillation during these months, which correspond to the cool season in that region.

The amplitude of the tropical pressure and central Pacific SST anomalies associated with the Southern Oscillation appear to be just as large and the relationships between them just as coherent during positive excursions of the Southern Oscillation (cold episodes) as during negative excursions (warm episodes).

Lead/lag relationships among climatic variables associated with the Southern Oscillation and El Niño events along the South American coast are also examined in the context of the same seasonal stratification. Our results are generally consistent with the traditional view that the Southern Oscillation is, to first order, a standing oscillation with geographically fixed nodes and antinodes.

1. Introduction

The concept of the Southern Oscillation and El Niño as manifestations of a single phenomenon involving fluctuations in the coupled atmosphere/ocean climate system is suggested in Berlage (1957) and in the influential papers of Bjerknes (1966, 1969), and is argued more explicitly in subsequent works, culminating in the extensive observational study of Rasmusson and Carpenter (1982; hereafter denoted as RC), which has come to be regarded as the definitive description of a canonical El Niño/Southern Oscillation (ENSO) warm episode. The results presented in that paper are based upon a composite of six warm episodes, characterized by pronounced positive sea surface temperature (SST) anomalies along the ship track just off the coast of Peru between 4° and 12°S. The anomalies appear to be phase locked to the annual cycle, reaching a maximum between April and June. For the sake of convenience, we will refer to the calendar years in which these episodes occurred as warm years. Five main features emerged in the RC composite, all of which are deeply rooted in the El Niño/Southern Oscillation literature:

i) El Niño events; i.e., strong positive SST anomalies in the eastern equatorial Pacific and along the South American coast from the equator to about 12°S, reaching a maximum along the Peruvian coast around May. As noted by Wyrtki (1975) and RC, there is a tendency for a second peak in SST at the coastal stations around December of a warm year, which sometimes persists into the first month or two of the subsequent calendar year.

ii) Weaker, but spatially coherent warming of SST, extending across the entire equatorial Pacific eastward of 170°E, gradually building up throughout the year to a peak around December. This basin-wide warming is to be distinguished from (i) both on the basis of zonal scale and timing.

* Present affiliation: Max Planck Institute for Meteorology, Hamburg, Federal Republic of Germany.

Corresponding author address: Professor John M. Wallace, Dept. of Atmospheric Sciences, AK-40, University of Washington, Seattle, WA 98195.

iii) A negative swing of the Southern Oscillation, which denotes a partial or total collapse of the east–west sea level pressure gradient across the tropical South Pacific, with positive sea level pressure anomalies at Darwin and negative pressure anomalies at stations in the southeast Pacific, reaching a peak around September of a warm year.

iv) A shift of the belt of heavy rainfall, normally located over Indonesia, eastward into the central Pacific beginning in April or May and reaching its maximum extent near the end of the year. The resulting extended episodes of heavy rainfall are a distinctive climatic feature of the desert islands of the equatorial Pacific (Doberitz 1968; Taylor 1973). The eastward shift of the rain belt is evident not only in rainfall data, but also in infrared satellite imagery (e.g., see Heddinghaus and Krueger 1981; and Liebmann and Hartmann 1982).

v) Westerly surface wind anomalies over the equatorial western Pacific near and to the west of the region of anomalously heavy rainfall, reaching peak intensity late in the year.

Barnett (1983, 1984a,b, 1985) has shown that warm episodes in the equatorial Pacific are also accompanied by wind and pressure fluctuations over the tropical Indian Ocean. His analysis suggests that the pressure and zonal wind perturbations associated with the Southern Oscillation originate over the tropical Indian Ocean and propagate eastward into the western and central Pacific over the course of about a year. The recent analysis of tropical upper air data by Gutzler and Harrison (1987) also emphasizes the eastward propagation of zonal wind anomalies.

In the present study, we reexamine the El Niño/Southern Oscillation phenomenon from a somewhat different perspective from RC and Barnett. As in RC, we use the months and seasons of the calendar year as a basis for stratifying the data relative to warm episodes in the equatorial Pacific. In this sense, many of our results are directly comparable to theirs. However, whereas RC keyed their composite to El Niño events along the South American coast, our analysis is based on sea level pressure anomalies at Darwin, the western pole of the Southern Oscillation. Hence, our analysis scheme, described in section 2, places relatively more emphasis upon conditions in the western Pacific and Indian Ocean sectors, and less upon conditions in the eastern Pacific. We will be interested in seeing how much the difference in regional emphasis in the analysis scheme affects the results. In contrast to RC who relied upon compositing techniques, and Barnett (1983, 1984a,b, 1985) and Gutzler and Harrison (1987) who relied upon complex empirical orthogonal functions, we use simple linear correlations and regressions as a quantitative measure of the strength of the relationships between the various climatic variables. Results, many of which are extracted from a more extensive compilation of statistics in Wright et al. (1985), are presented in sections 3 and 4. As a test of the validity of our approach, we examine, in section 5, the extent to which the relationships associated with the Southern Oscillation are nonlinear, with warm episodes being more distinctive than the intervening colder periods. The final discussion section includes a simultaneous cross-correlation matrix for a selection of the primary variables involved in the El Niño/Southern Oscillation phenomenon.

2. Analysis scheme and data

The analysis of the Southern Oscillation in sections 3 and 4 is based on correlation and regression statistics built around a common reference time series. As the reference variable we have used an index based on Darwin sea level pressure in preference to the widely used Southern Oscillation Index (SOI) based on the pressure difference between Tahiti and Darwin (e.g., see Trenberth 1976b, 1984) in order to minimize the amount of structure imposed upon the spatial correlation patterns through our choice of reference variable. A strong Southern Oscillation signal is evident in spatial correlation patterns based on Darwin alone. Note that the year-to-year fluctuations in Darwin pressure are of opposite polarity to those of most conventional Southern Oscillation indices, which are defined such that positive values denote an abnormally strong Pacific tradewind circulation.

The time series of our Darwin Pressure Index (DPI) contains 30 elements, one assigned to each calendar year starting with 1950 and ending with 1979. The value for a given calendar year is the average of the mean sea level pressures for the 12 consecutive months, beginning with April of that year and ending with March of the following year. We departed from the conventional calendar year in recognition of the strong seasonal dependence of month to month autocorrelation of pressure anomalies at Darwin: in the 1950–79 record the 1-month lag correlations range from 0.79 for September/October to 0.30 for March/April. Defining the Darwin year as extending from April through March maximizes the temporal variance of the index and, equivalently, minimizes the variance of monthly mean pressures about the index. Values of the DPI for the period 1950–79 are shown in Fig. 1 and listed in Table 2. We have found that the strong relationships during the core of the Darwin year, July through November, can be reproduced using the simultaneous seasonal mean Darwin pressure anomalies in place of the DPI.

The DPI was correlated with seasonal mean values of sea level pressure, sea surface temperature, and the zonal and meridional wind components, starting with the June–August mean for the previous calendar year, denoted by JJA_{-1}, followed by the consecutive 3-month seasons SON_{-1}, DJF_0, MAM_0, JJA_0, SON_0, DJF_1 and MAM_1, where the final season corresponds to March–

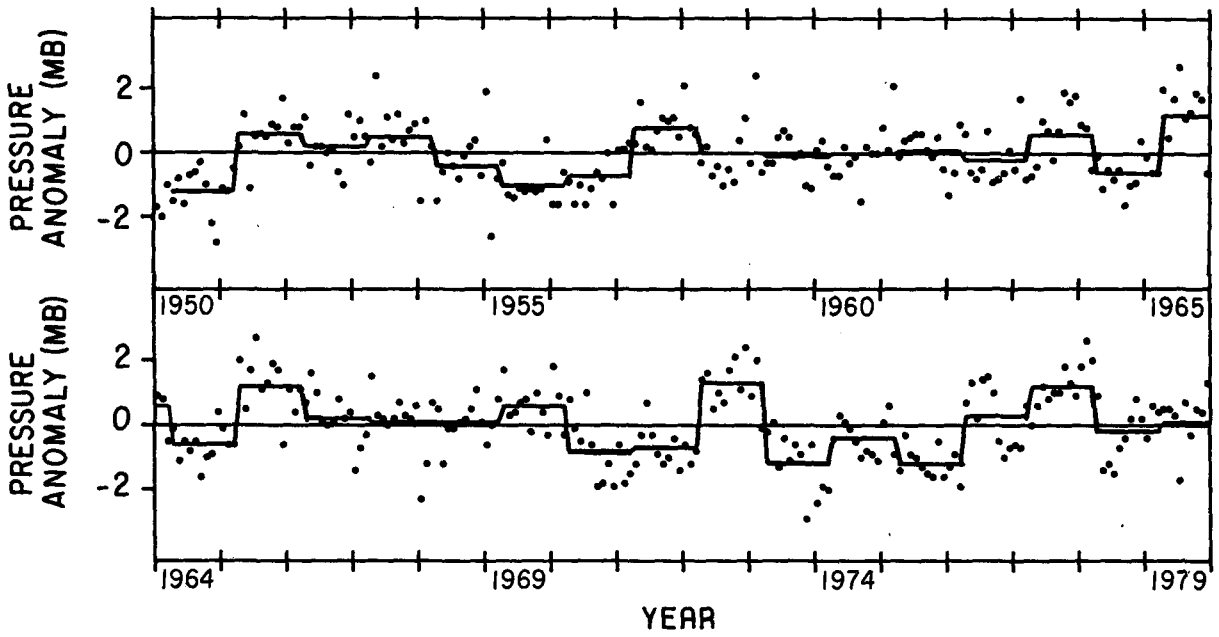

FIG. 1. Time series of Darwin monthly pressure anomalies (dots) and the DPI (solid line). The DPI is a 12-month average (April through March) of Darwin monthly pressure anomalies.

May of the calendar year following the year of the DPI, as illustrated schematically in Fig. 2. By correlating each of the elements in the above sequence of seasonal mean fields with the same 30-point time series of the DPI, we obtained a sequence of maps analogous to the RC composite maps. The resulting fields may be displayed either as regression maps or, in fully normalized form, as correlation maps.

Taking into account the 1-year autocorrelation of the DPI during the 1950–79 period of record (−0.2), correlation coefficients with absolute values of 0.40, 0.51, and 0.62 correspond to the 95%, 99% and 99.9% a priori significance levels, respectively, for a time series 30 yr in length. The true a posteriori significance levels are, of course, much lower, and it is not obvious to us how to estimate them accurately. We will restrict our attention to those features whose correlation with the DPI exceeds 0.7 in absolute value and/or were emphasized by RC or Barnett (1983, 1985). Regression coefficients are expressed as anomalies (in dimensional units) of the variable in question, per millibar anomaly of the DPI. Coincidentally, the regression coefficients expressed in these units have numerical values comparable to the actual anomalies observed during moderately strong swings of the Southern Oscillation, for which the DPI is of order unity. (The index exceeded 1.0 mb only in 1965, 1972, and 1977 and it was below −1.0 mb only in 1950, 1955, 1973 and 1975.) We have applied the above analysis scheme to the following datasets:

i) The Comprehensive Ocean-Atmosphere Data Set (COADS), based on observations from ships of opportunity over the entire world ocean, described in Fletcher et al. (1983). The COADS contains gridded, monthly mean fields of pressure, SST, and the zonal and meridional wind components together with auxiliary fields documenting the number of individual observations upon which each monthly mean statistic is based. The data are archived in 2° × 2° latitude–longitude grid boxes by individual year/month.

ii) Sea level pressure and rainfall data obtained from

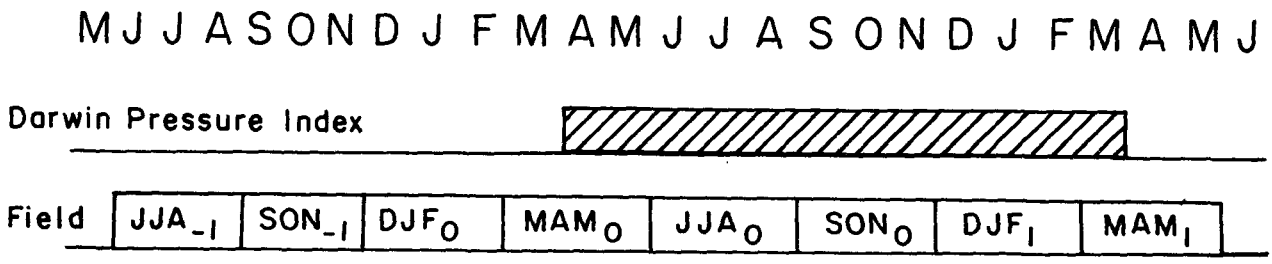

FIG. 2. Averaging intervals used in this study.

the World Monthly Surface Station Climatology (WMSSC) dataset.

iii) Monthly mean, gridded sea level pressure fields for the entire Northern Hemisphere produced by the U.S. Navy Fleet Numerical Weather Central (FNWC). In contrast to the COADS pressure data, in which the original ship based observations were binned on a monthly basis for 2° × 2° latitude–longitude grid squares and then averaged, the FNWC data were analyzed in an operational environment, and the resulting gridded values were archived on a daily basis, from which monthly averages were later computed.

iv) Puerto Chicama SST (Rasmusson, personal communication).

Datasets (1), (2), and (3) are available on digital tape from the NCAR Data Library. We will now describe the preprocessing of the datasets.

a. COADS

A climatological monthly mean was calculated for each variable, calendar month, and 2° × 2° latitude–longitude region, provided that at least 10 of the 30 yr contributed to the mean. A simple smoothing, interpolation, and extrapolation procedure was then applied to the climatology to enhance the coverage and representativeness of the climatology. Anomalies for the 2° × 2° latitude–longitude regions were calculated by subtracting from each monthly mean the corresponding climatological mean for that month. The 2° × 2° anomalies were then averaged, weighted by the number of observations, to form 4° × 10° latitude–longitude regional anomalies, and these monthly anomalies averaged in time to form seasonal anomalies. Further details of this calculation can be found in Wright et al. (1985). The results presented here do not appear to be sensitive to the details of the anomaly calculation.

For each 4° × 10° grid box in each field and for each of the eight seasons relative to the 12 months of the DPI (Fig. 2), a correlation coefficient and a regression coefficient were calculated. Coefficients were calculated only for 4° × 10° areas with at least 10 yr of data. A complete selection of charts for six of these seasons (all except JJA_{-1} and SON_{-1}) is presented in Wright et al. (1985), as numerical values. Except as otherwise noted, regions of insufficient data (based on the above criteria) are omitted from the analyses.

b. Navy pressure grids

The FNWC data consist of daily, objectively analyzed pressure fields for the Northern Hemisphere (0°–90°N) for the period 1950–1977 (Jenne 1975). The daily data, on a 63 × 63 grid, were averaged to form monthly means and then interpolated onto a 2.5° × 5° latitude–longitude grid. Monthly mean climatological charts were then prepared for the years 1950–77, and these charts were used as a basis for generating monthly anomaly charts. The monthly anomalies were averaged in time to form seasonal anomalies on the 2.5° × 5° grid, which were correlated with the DPI.

c. Rainfall data

The rainfall data extracted from the WMSSC tape were processed according to the method used by Meisner (1976), RC, and Rasmusson and Carpenter (1983). First, the monthly rainfall totals for each station were averaged into 3-month seasons for the period 1950–79. Then seasonal percentile ranks were computed for each seasonal value for each station. For example, the wettest (driest) winter, spring, summer and fall during 1950–79 were each assigned a value of 100 (1). Then the seasonal ranked station data were grouped on the basis of location and similarity (as determined by a visual inspection of the time series) and averaged to form regional indices. Finally, the seasonal values of the indices were assigned percentile ranks so that the values range from 1 to 100, regardless of the number of contributing stations. The number of stations grouped together in these indices ranges from 1 to 11. A listing of the 126 rainfall stations used in the study is available, upon request, from the authors.

3. Correlation and regression fields

a. Pressure and wind

Correlation and regression maps based on the DPI were generated from seasonal mean data for eight consecutive seasons starting with JJA_{-1}, as explained in section 2. Highlights of the results for the first three seasons (not shown) can be summarized as follows.

SON_{-1} marks the first appearance of correlation coefficients in excess of 0.5 in absolute value. In agreement with results of Trenberth (1976a), van Loon and Shea (1984, 1987), Gordon (1986), and Trenberth and Shea (1987), pressure in the Tasman Sea is negatively correlated with the DPI during JJA_{-1} and SON_{-1}, with strongest correlations reaching −0.65 in SON_{-1}. The lack of reproducibility of this feature in the analysis of an earlier period of record (see Table 1) discouraged us from pursuing it further in this analysis. For evidence which supports the statistical significance of this feature, see Trenberth and Shea (1987).

In agreement with RC, the weakening of the subtropical anticyclone in the southeast Pacific is evident in DJF_0: pressures in that region exhibit correlations with the DPI on the order of −0.5. Pressure anomalies over the Indian Ocean do not become significant until MAM_0, when correlations jump to around +0.7 over a broad region extending from the Arabian Sea to Indonesia. These pressure changes are accompanied by the appearance of zonal wind anomalies over the western and central equatorial Pacific.

Figure 3 shows sea level pressure regression contours for four consecutive seasons, beginning with JJA_0, to-

TABLE 1. Correlation between SON_{-1} pressure and the Darwin pressure index.

Period of record	Melbourne (38°S, 145°E)	Sydney (34°S, 151°E)	Auckland (37°S, 175°E)	Chatham Island (44°S, 176°E)
1950–1979	−0.50	−0.52	−0.66	−0.45
1900–1949	0.01	0.04		
1916–1949			0.00	
1930–1949				0.16

gether with wind vectors scaled in proportion to their respective regression coefficients. The corresponding correlation coefficients for the sea level pressure field (SON_0 and DJF_1 only) are tabulated in Fig. 4.

The patterns for MAM_0 (not shown) and JJA_0 are similar. During JJA_0 the pressure and wind anomalies near the eastern pole of the Southern Oscillation reach their peak values, with correlation coefficients with the DPI on the order of −0.8 for pressure in the tropical eastern and subtropical southeastern Pacific (Wright et al. 1985; Fig. 18a). In agreement with RC, we find a well-defined pattern in the wind regressions, with anomalous meridional flow toward the equator in both hemispheres from the dateline eastward, and westerly wind anomalies along the equator throughout the western and central Pacific in years of above normal DPI.

The midpoint of the year of the DPI and the time of strongest pressure and wind anomalies in the Pacific and Indian Ocean sectors, in terms of both correlations and regressions, is marked by SON_0. The pressure pattern over the Indian Ocean is stronger than during the previous season, and it is bordered, along its western flank, by a coherent patch of equatorial zonal wind anomalies, opposite in polarity to those in the Pacific. The zonal wind anomalies in the western and central Pacific remain strong, while the pressure anomalies in the eastern Pacific diminish slightly relative to the previous season. Strong meridional wind anomalies are observed in the southern tropics over the central Pacific.

A strong pattern reminiscent of those of the previous seasons is exhibited in DJF_1. Positive pressure anomalies have developed in the subtropical western Pacific in both hemispheres, with correlation coefficients on the order of 0.8. The zonal pressure gradient along the equator near the dateline has tightened relative to the previous season and the regression coefficients of the zonal wind anomalies in this region have increased to almost 2 m s^{-1} per mb. The patch of zonal wind anomalies of opposite sign farther to the west has weakened relative to the previous season and it has shifted eastward and intruded into the extreme western Pacific. Pressure anomalies over the tropical eastern Pacific have continued to weaken.

In MAM_1, vestiges of the equatorial zonal wind anomalies are observed along the ship track at 160°W but the corresponding correlation coefficients have dropped to about +0.3. The patch of zonal wind anomalies over the Indian Ocean and Indonesia during the previous seasons has shifted eastward into the western Pacific. However, the correlations associated with this feature have weakened to about −0.5.

As a check on the pressure anomalies derived from the COADS, we calculated correlation and regression coefficients between the DPI and seasonally averaged pressure anomalies derived from the U.S. Navy FNWC dataset. Figures 4a and 4b show contours of the correlation coefficients derived from the FNWC data overlaid upon the numerical values from the COADS for SON_0 and DJF_1, respectively. The agreement between the two sets of statistics is remarkably good, considering the fact that they have been analyzed in a completely different manner as explained in section 2.

b. Sea surface temperature

The regression maps for SST (Wright et al. 1985; Figs. 10–15, not reproduced here) are very similar to those for the RC composite, not only in terms of spatial pattern, but, fortuitously, even in terms of numerical values. Correlations between SST and the DPI are strongest for the equatorial central Pacific, slightly weaker for the equatorial eastern Pacific, and weaker still for the El Niño region along the Peruvian coast. In JJA_0, SON_0, and DJF_1, correlations with the DPI are as high as +0.9 for the central Pacific and +0.8 for the eastern equatorial Pacific. The corresponding correlations along the Peruvian coast (the region corresponding to shiptrack 1 of RC) are on the order of +0.6 in MAM_0, the season of El Niño events, and reach maximum values of about +0.7 from JJA_0 through SON_0. The relationships for stations along the Peruvian coast are comparable in strength to those for the Offshore index.

RC identified an elongated region of below normal SST extending eastward from Indonesia along the southern flank of the South Pacific convergence zone. This feature is apparent in our analysis, with correlation coefficients as strong as −0.7 in SON_0.

c. Rainfall

Figure 5 shows correlations between the DPI and precipitation (ranked and grouped as described in section 2c) for four successive seasons starting with JJA_0. Positive correlations are observed at stations in the

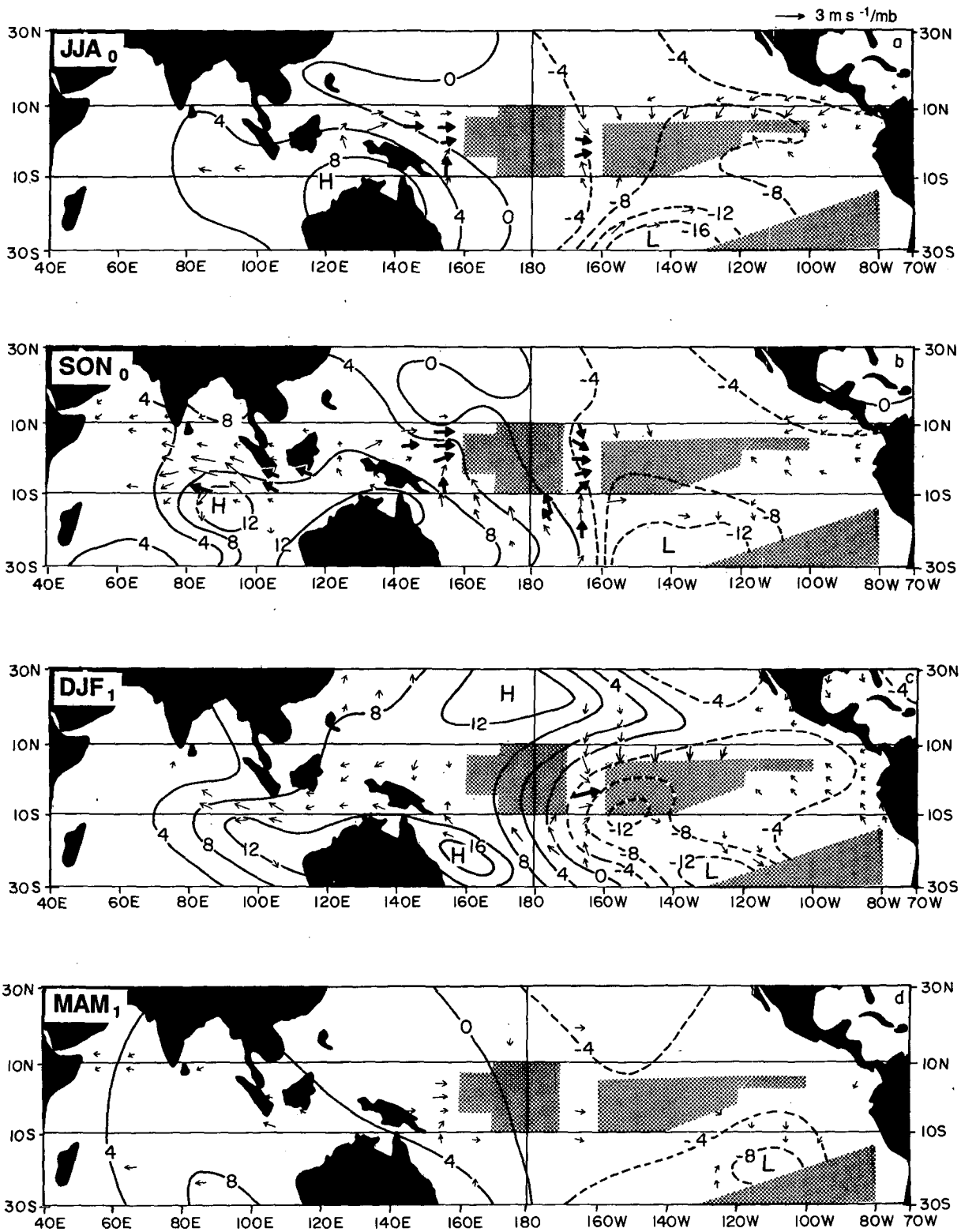

FIG. 3. Regressions of seasonal pressure and vectorial surface wind anomalies on the DPI for (a) JJA_0, (b) SON_0, (c) DJF_1, and (d) MAM_1. Solid contours indicate pressure anomalies (in tenths of millibar) per millibar pressure anomaly of the DPI. Wind vectors are shown only for those grid points whose u or v correlations with the DPI exceed 0.5 in absolute value and thick arrows denote u or v correlations in excess of 0.7 in absolute value. Pressure regression contours have been manually interpolated across the shaded data-void regions.

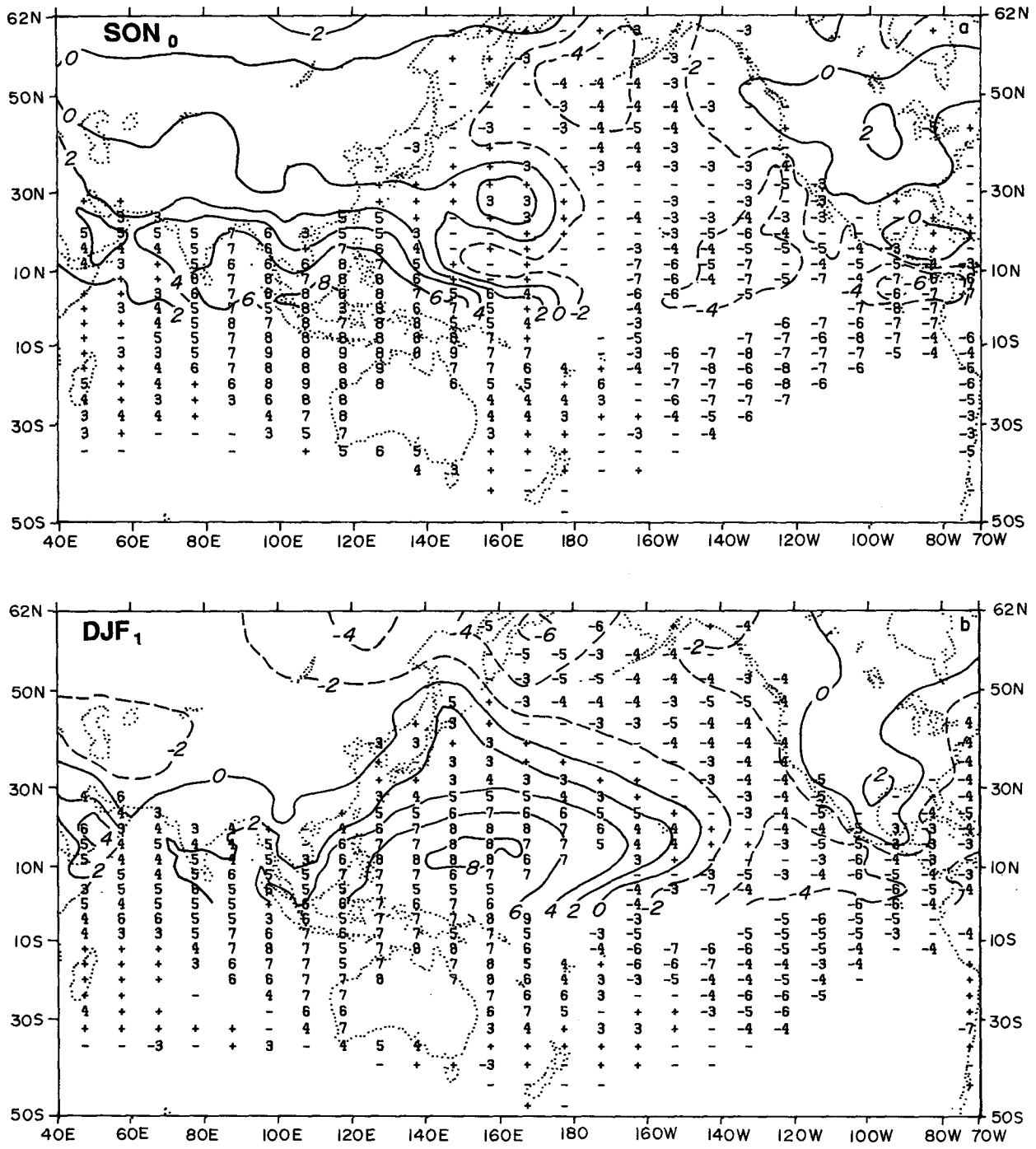

FIG. 4. Correlation coefficients (×10) between the DPI and COADS pressure (digits) and between the DPI and FNWC pressure (contours) for (a) SON_0 and (b) DJF_1. The FNWC data are for the Northern Hemisphere only. Contour interval is 2. Correlation coefficients between 2 and −2 for the COADS are shown by sign only.

equatorial dry zone in the central Pacific reaching values as high as +0.9 during SON_0, indicative of enhanced rainfall during warm episodes. The region of positive correlations is flanked on the north, south, and west by a horseshoe-shaped region of somewhat weaker negative correlations, indicative of suppressed rainfall during warm episodes. Much of this region also experiences significantly less cloudiness than normal during warm episodes (Wright et al. 1985). Further details of the timing of the anomalous precipitation over the tropical Pacific are discussed in the next section.

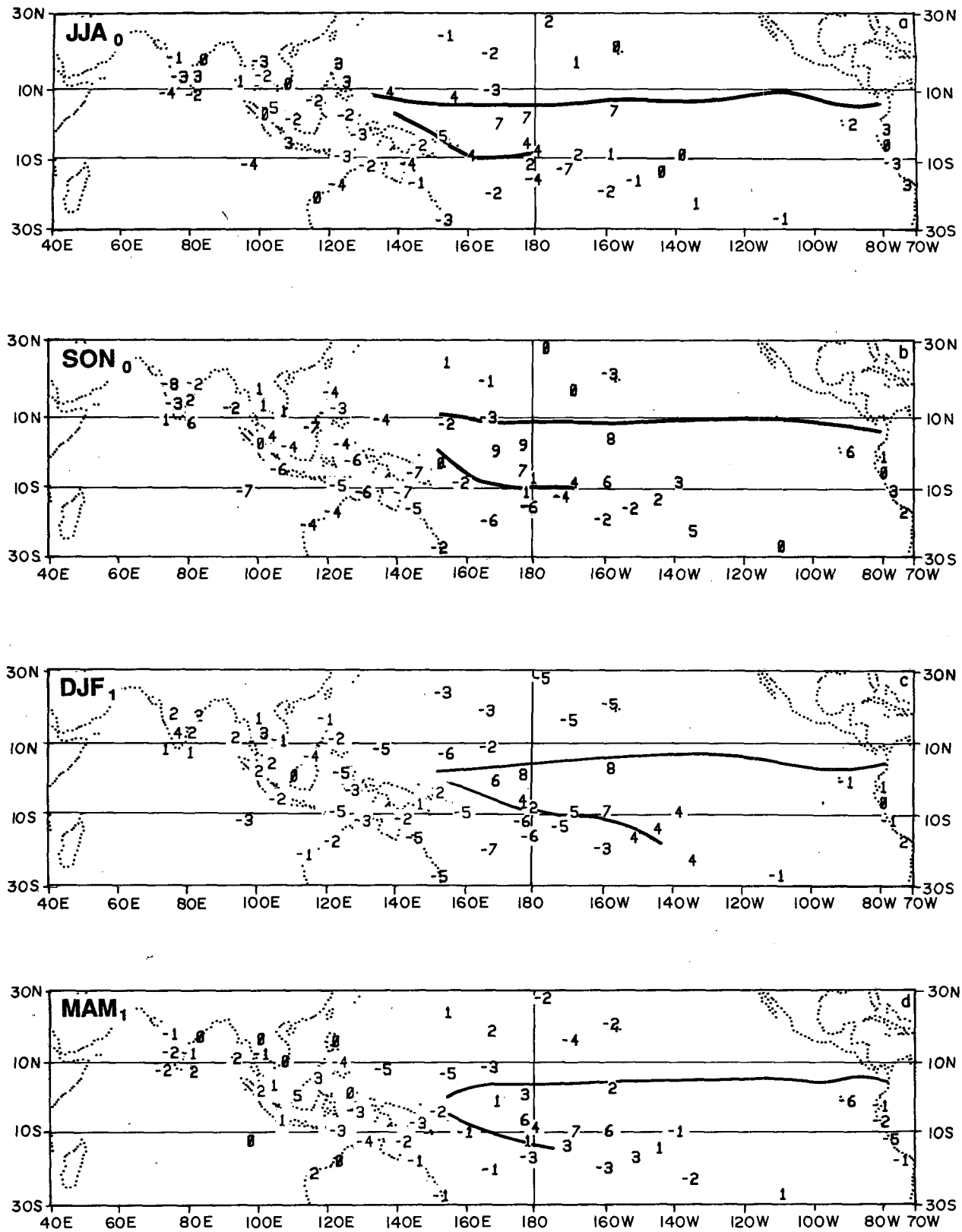

FIG. 5. Correlation coefficients (×10) between the DPI and seasonal rainfall indices for (a) JJA_0, (b) SON_0, (c) DJF_1, (d) MAM_1. The rainfall indices are constructed from percentile ranks of seasonal rainfall totals at several island stations; see section 2c for details. Heavy lines indicate the climatological mean axes of the ITCZ and SPCZ, as given in Taylor (1973).

Consistent with results of Mooley and Parthasarathy (1983) and Rasmusson and Carpenter (1983), rainfall over India during the summer monsoon season tends to be suppressed during years of positive DPI, but the correlations are not as strong as we had expected on the basis of previous works. In agreement with Rasmusson and Carpenter (1983) and Ropelewski and Halpert (1987), stations on Sri Lanka experience above normal rainfall during their rainy season SON_0, with somewhat stronger correlations than those over India.

Rainfall at the Galapagos Islands and along the South American coast does not exhibit a strong and consistent relationship with the DPI. However, Galapagos Islands and Guayaquil, Ecuador (2°S) rainfall and Piura River (5°S) stream flow in Peru during the January–May rainy season exhibit strong positive correlations with local SST and negative correlations with local pressure (not shown).

4. Correlation statistics for selected regions

In order to show more clearly the evolution of the features described in the previous section, we generated a set of indices by averaging monthly anomalies of selected parameters within specified geographical regions, shown in Fig. 6, in which the signals described in section 3 are most clearly defined. The regional pressure indices were calculated from normalized monthly anomalies so that all grid boxes would have equal weight in the spatial averages. Monthly values of the indices were temporally smoothed with one pass of a three-point binomial filter. Correlation and regression coefficients between each smoothed monthly regional index and the DPI were calculated for each of the 21 months starting 7 months before the beginning of the year of the DPI and continuing for 2 months after the end of the year of the DPI (see Fig. 2). The resulting time series of lag correlation and regression coefficients describe the time dependent relationships between the regional indices and the DPI.

a. Sea level pressure

Figure 7 shows lag-correlations for sea level pressure over selected regions in the Indian and Pacific sectors, as indicated. As expected, Darwin, itself, exhibits the strongest correlation with the DPI, with correlation coefficients above +0.8 from May through February and above +0.9 from August through October. Tahiti exhibits an out of phase relation with Darwin, with negative correlations on the order of −0.8 from July through October. The negative correlations between the DPI and the higher latitude stations Rapa and Easter are not so strong as those for Tahiti and the lag correlation functions are rather noisy in appearance. The lag-correlation function for our southeast Pacific pressure index for the ship track to the northwest of Easter Island resembles the one for Tahiti, but it leads Tahiti by about 2 months. The intriguing 6-month phase lag noted by Quinn (1974, 1979), Trenberth (1976a), Chen (1982) and Trenberth and Shea (1987) between the pressure falls in the southeast Pacific and subsequent pressure rises at Darwin is apparent in these data, but levels of correlation are modest in comparison to the simultaneous correlations.

Figure 7 also shows lag-correlations between the DPI and a regional pressure index for the eastern half of the Indian Ocean between 10°N and 22°S (see Fig. 6), near the western pole of the Southern Oscillation. The Indian Ocean index leads the DPI by about a month during both the upswing in the correlations, around March of the Darwin year, and during the downswing about a year later. In March and April of the Darwin year, the Indian Ocean pressure index is more strongly correlated with the DPI than is Darwin pressure itself. The correlations weaken slightly during the northern

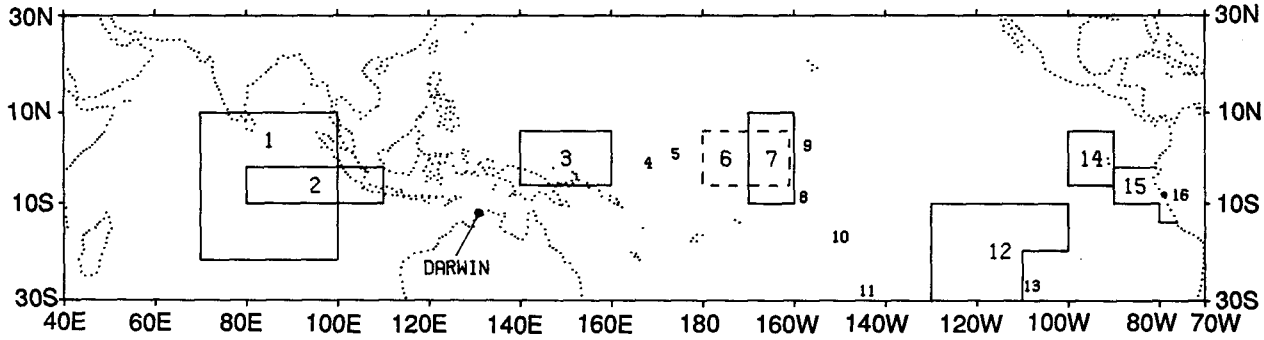

FIG. 6. Regional indices defined in this study and station locations: 1) Eastern Indian Ocean pressure (10°N–22°S, 100°–70°E), 2) Indian Ocean zonal wind (2°–10°S, 110°–80°E), 3) Western Pacific zonal wind (6°N–6°S, 160°–140°E), 4) Nauru/Ocean rainfall (1°S, 168°E), 5) Gilbert Island rainfall (1°N, 174°E), 6) Central equatorial zonal wind (6°N–6°S, 180°–160°W), 7) Central Pacific SST (10°N–10°S, 160°–170°W), 8) Eastern Tokelau Island rainfall (9.5°S, 160°W), 9) Line Island rainfall (2.9°N, 158°W), 10) Tahiti pressure (17°S, 150°W), 11) Rapa pressure (28°S, 144°W), 12) Southeast Pacific pressure (10–20°S, 100°–130°W, and 20°–30°S, 110°–130°W), 13) Easter Island pressure (27°S, 109°W), 14) Eastern equatorial Pacific SST (6°N–6°S, 90°–100°W), 15) Peru Offshore SST (2°–14°S, coast–90°W), 16) Puerto Chicama SST (8°S).

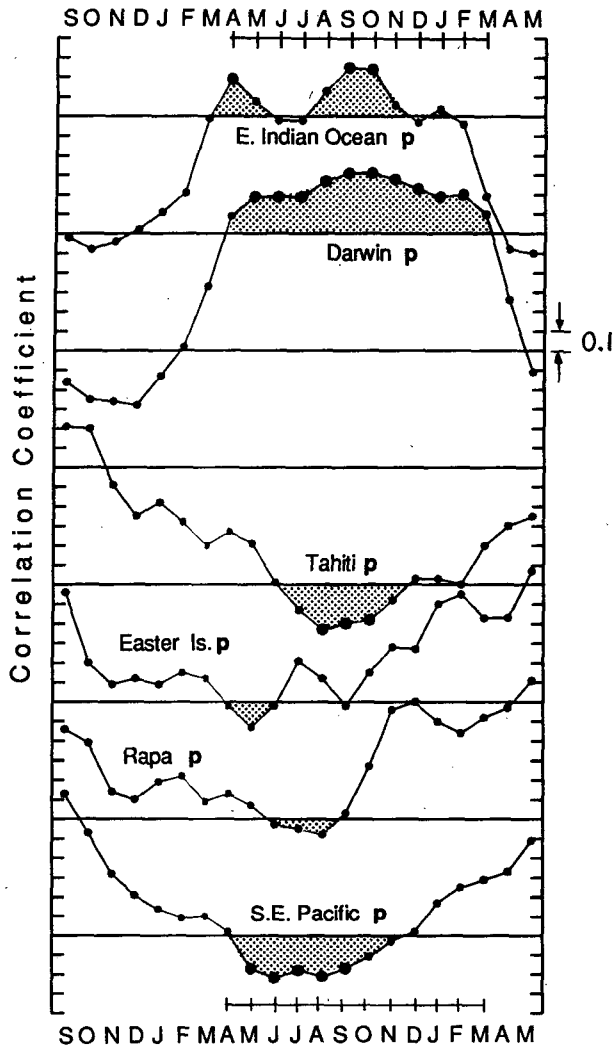

FIG. 7. Lag correlation coefficients between sea level pressure time series, as indicated, and the DPI. See Fig. 6 for locations of the indices. The 12 months used to construct the annual DPI are indicated by solid lines below the monthly labels at the top and bottom. Shaded segments denote correlation coefficients stronger than 0.6 in absolute value; large dots denote correlation coefficients greater than 0.8 in absolute value. Horizontal lines mark the −0.6, 0.0, and +0.6 correlation levels for each curve. Each successive curve is plotted at 0.6 units below the previous one: i.e., the zero correlation line for the first curve coincides with the 0.6 correlation line for the second curve, etc.

summer monsoon season, June–July, and then rise to a second peak in September–October.

b. *Sea surface temperature*

We defined three Pacific Ocean SST indices: central Pacific (10°N–10°S, 170°–160°W), eastern Pacific (6°N–6°S, 100°–90°W), and Peru Offshore (2°–14°S, eastward of 90°W), as shown in Fig. 6. We also used SST data for Puerto Chicama (8°S) on the Peruvian coast. Figure 8a shows lag correlations between the DPI and the four SST indices. Correlation coefficients first exceed +0.6 near the Peruvian coast in March, near the Galapagos Islands in May, and in the central Pacific in June. This westward progression of the onset of strong SST correlations is analogous to the westward spreading of warm SST anomalies in the RC composite. All four SST indices remain well correlated with the DPI for 10–11 consecutive months. The correlation coefficient between the central Pacific SST index and the DPI exceeds +0.9 from August to December. By July of the following year, the three eastern Pacific SST indices show substantial negative correlations with the DPI (−0.6), whereas the central Pacific SST index shows only a weak correlation with the DPI. The tendency for cold SST anomalies in the eastern Pacific in the year following a warm episode was noted by RC.

During some of the stronger warm episodes in this period of record (e.g., 1957–58, 1972–73), SST anomalies along the Peruvian coast reached a first maximum in April–June and a second maximum around November–December (Wyrtki 1975; RC). This double maximum is not evident in the lag correlations for Puerto Chicama, or in those for Talara (4°S) and La Punta (12°S) (not shown). However, the corresponding lag regression coefficients between the Puerto Chicama SST anomalies and the DPI, shown in Fig. 8b, clearly exhibit the double maximum. The magnitudes of the two regression peaks are comparable, even though the April–June correlations are lower, because coastal SST exhibits more interannual variability during April–June than during November–December (see Deser and Wallace 1987; their Fig. 1 and the accompanying discussion). It is interesting to note that the lag regressions for the Peru offshore SST index show a single peak in June, while those for the eastern Pacific index show a hint of the double maximum. The lag regressions for the central Pacific index show a single broad peak from September to December. These results are generally consistent with the RC warm event composite of SST along the cross-equatorial shiptracks.

c. *Central Pacific rainfall and SST*

Figure 9 shows lag correlations between the DPI and four western and central Pacific rainfall indices: Nauru and Ocean Islands (1°S, 168°E), the Gilbert Islands (1°N, 174°E), the Line Islands (3°N, 158°W), and the eastern Tokelau Islands (10°S, 160°W). Correlations between the DPI and the Nauru/Ocean, and Gilbert Islands indices reach +0.9 for several months in a row. As noted by RC, the heavy rainfall in association with warm episodes occurs a few months earlier at Nauru/Ocean than at the Gilbert Islands, about 8° of longitude farther east. This phase lag could be interpreted as evidence of the eastward propagation of the precipitation anomalies, consistent with patterns of anomalies in outgoing radiation observed during some of the more recent warm episodes (e.g., see Meehl 1987). However,

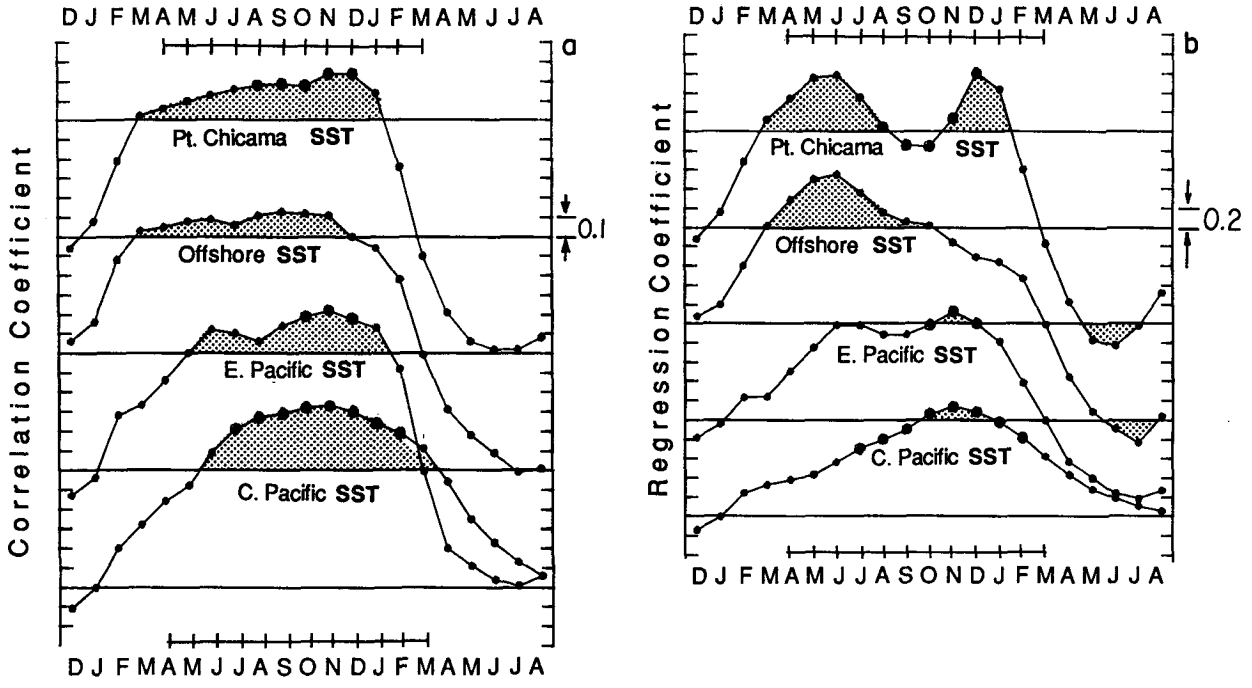

FIG. 8. (a) As in Fig. 7 but for Puerto Chicama, Peru Offshore, eastern equatorial and central equatorial Pacific SST. (b) The corresponding lag regression coefficients. Large dots indicate the months for which the corresponding correlation coefficients exceed 0.8 in absolute value (see Fig. 7). Horizontal lines are drawn at intervals of 1.0 K per mb anomaly in the DPI; the zero line of the first curve coincides with the 1.0 line for the second curve, etc. Regression coefficients greater than 1.0 K per mb anomaly in the DPI are shaded.

it should be noted that the rainfall anomalies in the Line Islands, 28° farther east, do not lag those in the Gilberts. The rainfall index for the eastern Tokelau Islands shows enhanced precipitation in association with warm episodes beginning late in the year of the DPI, much later than the rainfall indices to the north and west, and it extends well into the following year.

d. Time–longitude sections of wind and pressure

Figure 10 shows wind and pressure anomalies for the equatorial zone (10°N–10°S), as represented by a set of monthly indices computed at 10° longitude intervals for the Indian and Pacific sectors. The monthly mean pressure and winds were smoothed twice in time and once in the zonal direction with a three-point binomial filter. Lag correlation and regression coefficients between the DPI and the smoothed monthly pressure and wind indices were arranged to form longitude–time sections. To enhance the visual continuity of the diagrams, we linearly interpolated (in longitude) the monthly mean pressure data across data sparse regions (notably the central Pacific). Regions affected by the interpolation are indicated by light shading in the figures. We did not interpolate the wind field. Almost 2 yr of monthly lag regressions are shown, starting in the September before and continuing through the May after the year of the DPI (indicated by heavy lines along the left and right margins). Only those wind regression vectors whose correlations with the DPI exceed 0.5 in absolute value are plotted.

This section emphasizes the standing character of the Southern Oscillation. The onset of strong pressure anomalies around March of the year of the DPI is almost simultaneous in the equatorial Indian and eastern Pacific Oceans. The node of the zonal oscillation in pressure remains near the dateline throughout the period in which the pattern is strong, apart from a brief westward excursion during the summer monsoon season. The second half of the year of the DPI is marked by an eastward shift of the strongest pressure anomalies from the eastern Indian Ocean into the extreme western Pacific, together with the strongest westerly surface wind anomalies. The easterly wind anomalies over the Indian Ocean reach the western Pacific by the final months of the sequence but by that time the correlation coefficients have dropped below 0.5.

Figure 11a shows corresponding results for the northern subtropics (10°–30°N). (In this and in the following figure, pressure correlations are plotted in place of regressions and winds are not plotted.) In agreement with results of Barnett (1985; his Figs. 1 and 9), the pressure anomalies in this latitude belt exhibit more evidence of eastward propagation than those in the equatorial belt. Much of the eastward propagation takes place from September to December. During these

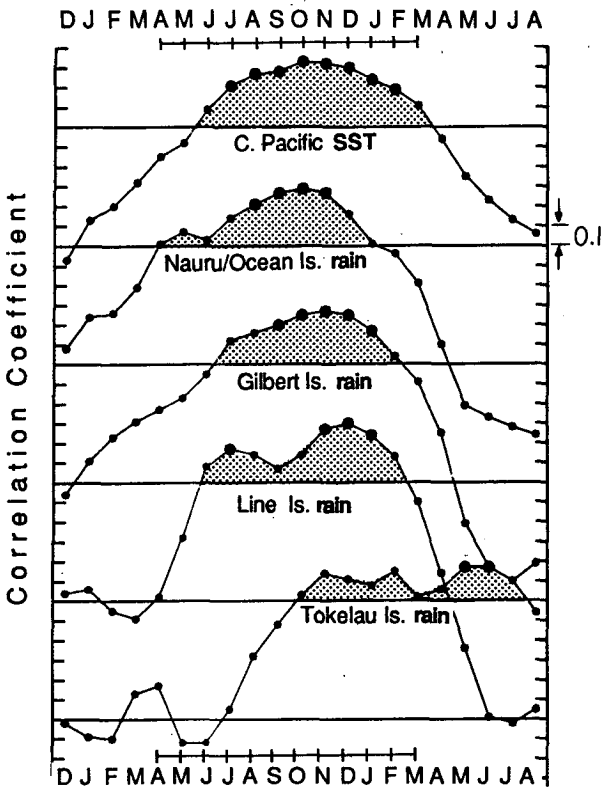

FIG. 9. As in Fig. 7 but for central equatorial Pacific SST and rainfall at Nauru/Ocean Islands, the Gilbert Islands, the Line Island, and the eastern Tokelau Islands. For approximate locations, see Fig. 6.

months, years of positive DPI are characterized by the rather sudden development of an anomalous subtropical surface anticyclone over the western Pacific, directly beneath the anomalous anticyclone that dominates the upper tropospheric circulation during the northern winter of warm episodes (Horel and Wallace 1981). This feature may be part of the barotropic response to anomalous convection over the central Pacific. During these same months the pressure anomalies diminish over the eastern Indian Ocean. These changes can be interpreted as the eastward propagation of the pressure signal associated with the Southern Oscillation, as suggested by Barnett, but they can equally well be viewed as a more discrete adjustment of the planetary wave pattern with the onset of the northern winter.

The corresponding section for the southern subtropics (10°–38°S) is shown in Fig. 11b. In October, preceding years of positive DPI, negative pressure anomalies prevail over the South Pacific between 150°E and the dateline. As noted above, this feature is much less pronounced in the record prior to 1950. At these southern latitudes the zonally oriented Southern Oscillation is evident in the pressure correlation field throughout the year of the DPI. There is a hint of eastward propagation of the western pole toward the end of the sequence, but the node in the pressure field shifts eastward by only about 15° of longitude through the course of the year over which the DPI is averaged. In all three sections the eastern pole of the Southern Oscillation attains its maximum strength about 5 months earlier than the western pole.

5. Summary of individual years, in ranked sequence

To document the degree of symmetry between years of high and low DPI, seasonal means of selected indices are listed by year in order of decreasing DPI in Table 2; the year and corresponding value of the DPI are also shown in the table. To simplify the display, the values of the seasonal indices are plotted in symbolic form, as indicated in the caption.

For each year, and for each index, means are displayed for six seasons: DJF_0, MAM_0, JJA_0, SON_0, DJF_1, MAM_1. These seasons are labeled according to the first letter of the central month: e.g., DJF_0 is denoted by J_0. Seasons in which the magnitude of the correlation between an index and the DPI is weaker than 0.6 in absolute value are shaded. Thus, the strongest Southern Oscillation signatures should be characterized by the clustering of plus symbols at one end and minus symbols at the other end of the unshaded portions of the tables. For details concerning the indices, see Fig. 6.

Those variables that are correlated with the DPI at a level of 0.8 or stronger for two or more consecutive seasons (e.g., Gilbert Islands rainfall and central equatorial Pacific SST) show virtually unbroken blocks of plus and minus signs in the extreme years in Table 2. Those variables with weaker correlations, such as SST in the eastern Pacific, exhibit less consistency.

It is evident from Table 2 that the anomalies in the indices display a coherent set of relationships, not only in years of high DPI near the top of the table, but also in years in which the opposite conditions prevail. The years 1950, 1975, 1955 and 1973 were distinctive for their strong pressure gradients across the Pacific and their cold SST and light rainfall in the central Pacific, just as 1972, 1965 and 1957 were distinctive for their anomalies in the opposite sense. Hence, it is apparent that both groups of years make roughly comparable contributions to the linear correlations examined in the previous sections.

The emphasis upon "warm episodes" in RC and in many other studies is based on the premise that they exhibit larger anomalies than the intervening "cold episodes." This is certainly true of SST along the Peruvian coast, which exhibits strong positive skewness (Deser and Wallace 1987). However, we have found that neither central Pacific SST nor Darwin pressure exhibit positive skewness. The lack of consistent positive skewness in the frequency distribution is further grounds for questioning whether warm (high DPI) years have any special significance relative to cold years.

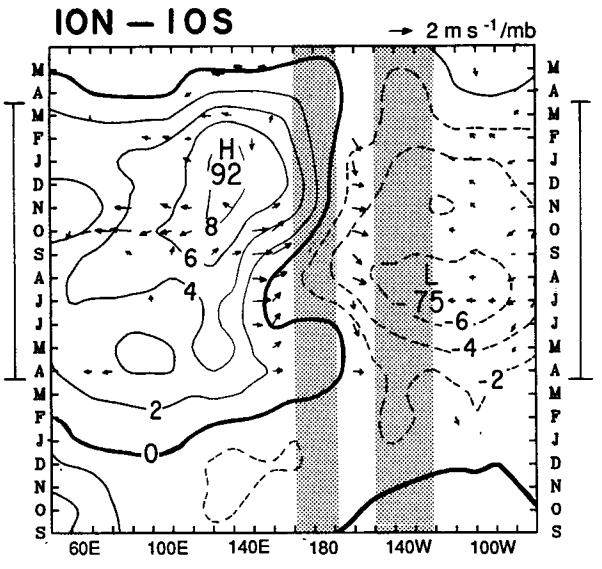

FIG. 10. Time–longitude plot of lag regression coefficients of monthly mean pressure and surface wind anomalies, averaged between 10°N and 10°S, on the DPI. The time axis runs upward starting with the September previous to and ending with the May following the year of the DPI. The 12 months used to construct the annual DPI are indicated by heavy lines at the left and right margins. Only those wind regression vectors for which the u or v correlations with the DPI exceed 0.5 in absolute value are plotted. Shading indicates data-void regions across which the pressure field has been interpolated. Contours in units of tenths millibar anomaly in pressure per millibar anomaly of the DPI, and the extrema labels are in hundredths millibar anomaly in pressure per millibar anomaly of the DPI.

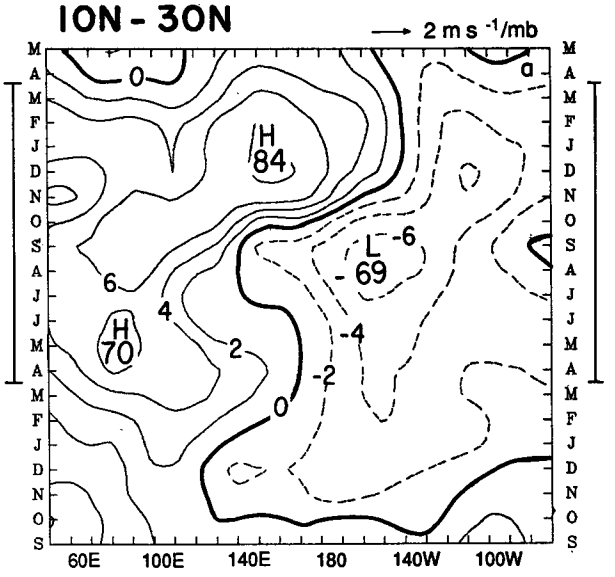

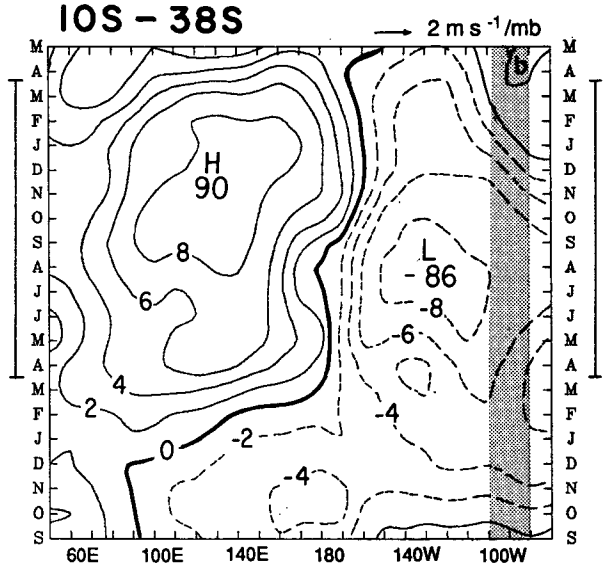

FIG. 11. As in Fig. 10 but pressure correlations (×10) are plotted in place of regressions; contour interval 2 and extrema labels are correlations (×100); wind vectors are omitted. (a) The latitude belt from 10°–30°N, and (b) the latitude belt from 10°–38°S.

6. Discussion

a. *Structure of anomalies during warm and cold episodes*

The correlation matrix shown in Table 3 provides a basis for summarizing the relationships involved in the canonical warm episode (or its mirror image cold episode) from the perspective of the Southern Oscillation. In this table we have included a selection of dynamically related equatorial indices ranging from the eastern Indian Ocean to the South American coast. The correlations are based on averages from July through November of each calendar year, which correspond to the middle months of the year over which the DPI is averaged and to the cool season in the eastern Pacific. The variables in the table include the five main features that emerged in the RC composite, as described in the Introduction, but for one important distinction: South American coastal SST refers to conditions about 4 months later than in the RC composite. Variables 1, 2, 3, 6 and 7 involve pressures, zonal pressure gradients, and zonal winds along the equator, which are related through the zonal equation of motion; 5 and 8 involve SST, which should be closely related to the pressure and wind fields hydrostatically and through the ocean dynamics; and 4 involves central Pacific rainfall, an indicator of vertical velocity which is linked to zonal wind through the continuity equation. For a definition of the variables listed in Table 3, see Fig. 6.

Nearly all the correlations in Table 3 exceed 0.7 in absolute value, the only marginal ones being those between Indian Ocean and eastern Pacific variables. The west to east pressure gradient across the Pacific, as indicated by 7 is even more strongly correlated with this set of equatorial variables than conventional Southern Oscillation indices based on pressure differences between Darwin and Tahiti (not shown). It is also note-

TABLE 2. Ranked chronology of selected indices of seasonally averaged variables. The years are arranged in order of decreasing DPI. For each year and each index, means are displayed for six consecutive seasons, DJF_0, MAM_0, JJA_0, SON_0, DJF_1, and MAM_1, labeled by the first letter of the central month. The large plus symbol denotes an anomaly more than one standard deviation above the climatological mean; small cross, between 0.5 and 1.0 standard deviations above the mean; solid circle, within 0.5 standard deviation of the mean, etc. The rainfall indices have been seasonally ranked and assigned the following symbols: large plus for top 15th percentile, small plus, top 15–30th percentile, short minus, bottom 15–30th percentile, large minus bottom 15th percentile. Blanks denote missing data. Shading indicates those seasons for which the magnitude of the correlation between the index and the DPI is weaker than 0.6. The indices are defined in Fig. 6 and discussed in section 4.

	DPI	CHICAMA	OFFSHORE	E EQ PAC	C EQ PAC	E INDIAN	DARWIN	SE PAC	C EQ PAC	NAURU–OCEAN	LINE IS.
	MB X 100	SST	SST	SST	SST	SLP	SLP	SLP	U	RAIN	RAIN
		$J_0A_0J_0Q_0J_1A_1$	$J_0A_0J_0Q_0J_1A_1$	$J_0A_0J_0Q_0J_1A_1$	$J_0A_0J_0Q_0J_1A_1$	$J_0A_0J_0Q_0J_1A_1$	$J_0A_0J_0Q_0J_1A_1$	$J_0A_0J_0Q_0J_1A_1$	$J_0A_0J_0Q_0J_1A_1$	$J_0A_0J_0Q_0J_1A_1$	$J_0A_0J_0Q_0J_1A_1$
1972	130										
1977	128										
1965	127										
1957	87										
1963	66										
1969	63										
1951	63										
1953	58										
1976	29										
1952	26										
1966	23										
1979	18										
1968	13										
1967	13										
1961	11										
1960	3										
1958	−3										
1959	−6										
1978	−18										
1962	−18										
1974	−36										
1954	−39										
1964	−59										
1971	−69										
1956	−70										
1970	−82										
1955	−98										
1975	−116										
1973	−116										
1950	−117										

TABLE 3. Correlation matrix between selected indices in the equatorial belt, based on averages from July–November for each of the 30 years 1950–79. The indices are arranged from west to east in the table and are as defined in Fig. 6. Correlations of 0.8 and above are printed in boldface type, except in the case of "built in" correlations.

	1 Indian Ocean zonal wind (110–80°E)	2 Darwin SLP (131°E)	3 West Pacific zonal wind (160–140°E)	4 Line Island rainfall index (160°W)	5 Central Pacific SST (170–160°W)	6 East Pacific SLP (110–90°W)	7 Darwin minus E. Equatorial Pacific SLP	8 Puerto Chicama SST
(1)	1.00	**−.84**	**−.86**	−.64	−.77	.61	−.79	−.61
(2)	**−.84**	1.00	**.88**	.78	**.88**	−.76	.95	**.80**
(3)	**−.86**	**.88**	1.00	**.84**	**.84**	**−.80**	**.90**	**.82**
(4)	−.64	.78	**.84**	1.00	.75	−.75	**.82**	**.90**
(5)	−.77	**.88**	**.84**	.75	1.00	−.78	**.90**	**.80**
(6)	.61	−.76	**−.80**	−.75	−.78	1.00	−.92	**−.86**
(7)	−.79	.95	**.90**	**.82**	**.90**	.92	1.00	**.88**
(8)	−.61	**.80**	**.82**	**.90**	**.80**	**−.86**	**.88**	1.00

worthy that the SST in the central equatorial Pacific bears more of a relationship to the Darwin pressure than to the pressure in the eastern Pacific, while the SST at Puerto Chicama is more strongly related to the local pressure.

Together with the correlation statistics presented in sections 3 and 4, these statistics serve to confirm the existence of coherent relationships among climatic variables over the tropical Pacific and Indian Ocean sectors, as summarized in the Introduction. The well-known Southern Oscillation signature is prominent in the pressure patterns derived from the COADS, with strong negative correlations between Darwin and pressures not only in the subtropical southeast Pacific, but also in the eastern equatorial Pacific. Similar relationships between the climatic variables considered in this study have been noted in a number of recent GCM sensitivity experiments (e.g., Blackmon et al. 1983; Shukla and Wallace 1983; Lau 1985; Palmer and Mansfield 1984, 1986a,b).

The simultaneous relationships among the variables listed in Table 3 are all considerably weaker during April–June, the season in which the SST anomalies associated with El Niño events along the Peruvian coast are most pronounced, than during July–November. For example, the correlation between central Pacific SST and the Darwin-east Pacific pressure difference drops from 0.90 in July–November to 0.54 in April–June, while the correlation between central Pacific SST and Puerto Chicama SST falls from 0.80 in July–November to 0.38 in April–June. However, Puerto Chicama SST remains well correlated (−0.80) with east Pacific pressure (and the east–west pressure difference) during April–June.

b. *Precursors*

In agreement with the studies cited in section 3a, we find evidence of pressure falls in the Tasman Sea area, two or three seasons in advance of the pressure rises at Darwin. The levels of correlation in the 1950–79 record are strong enough to suggest that this relationship might have some useful predictive value. However, when a longer period of record is considered (see Table 1), the correlations are less impressive.

In agreement with Quinn (1974), Trenberth (1976a), and Trenberth and Shea (1987), we find that pressure fluctuations in November–January over the eastern pole of the Southern Oscillation (Fig. 7) tend to precede Darwin pressure anomalies of opposite sign during the subsequent Darwin year, but these relationships are much weaker than those during the Darwin year. In our analysis, the pressure changes over the Indian Ocean that occur in association with the Southern Oscillation precede those at Darwin by only a month or 2.

c. *Zonal propagation*

Clearly, the dominant feature in our statistics is the planetary-scale standing wave pattern in the pressure field, first identified by Walker and Bliss (1932), and described in many subsequent studies. Whatever zonal phase propagation is evident in the lag-correlation statistics should be viewed as an embellishment upon this basic, underlying pattern, which is the dominant feature in Fig. 10. Whether phase propagation is essential to the mechanism of the Southern Oscillation remains to be seen.

Consistent with the results of RC, some tendency for westward progression of SST anomalies from the South American coast toward the central Pacific is evident in correlations based on Darwin pressure (Fig. 8b). However, the strongest correlations between the DPI and SST are observed during OND_0 at all longitudes from the coast westward to the central Pacific (Fig. 8a). Hence, the SST perturbations associated with the Southern Oscillation are closer to being simultaneous than one might infer from the RC composite. In view of the sharply contrasting time history of the 1982–83 warm episode in the eastern Pacific (Rasmusson and Wallace 1983), it remains to be seen

whether the subtle westward phase shift with time apparent in Fig. 8a will prove to be reproducible in independent datasets.

The eastward propagation of equatorial pressure and wind anomalies, emphasized by Barnett (1983, 1985) and prominent in the 1982/83 warm episode, is evident in our statistics, but the range of longitude over which it occurs is quite restricted and much of it appears to be associated with a rapid change in the pattern over the course of a few months at the time of onset of northern winter.

d. *Symmetry of the frequency distribution*

The examination of anomalies observed during individual years, presented in section 5, indicates that relationships with Darwin are, to first order, independent of the polarity of the Southern Oscillation. Furthermore, we find no evidence of positive skewness in Darwin pressure or central Pacific SST. These results justify, a posteriori, our use of linear correlations and regressions in lieu of compositing techniques in this study. However, it is interesting to note that Puerto Chicama and Offshore SST, and the Gilbert Islands zonal wind (173°–177°W) (not shown) exhibit strong positive skewness with largest anomalies during warm episodes. The amount of skewness present in these variables is not large enough to detract from the strength of the correlations.

Acknowledgments. We would like to thank the reviewers for their helpful comments and Kay Dewar for her assistance in preparing the figures. Peter Wright's participation in this paper was supported by the NOAA Equatorial Pacific Ocean Climate Studies (EPOCS) Program. Research of the other authors was supported under Grant 8318853 from the National Science Foundation's Climate Dynamics Program.

REFERENCES

Barnett, T. P., 1983: Interaction of the monsoon and Pacific trade wind system at interannual time scales. Part I: The equatorial zone. *Mon. Wea. Rev.*, **111**, 756–773.

——, 1984a: Interaction of the monsoon and Pacific trade wind system at interannual time scales. Part II: The tropical band. *Mon. Wea. Rev.*, **112**, 2380–2387.

——, 1984b: Interaction of the monsoon and Pacific trade wind systems at interannual time scales. Part III: A partial anatomy of the Southern Oscillation. *Mon. Wea. Rev.*, **112**, 2388–2400.

——, 1985: Variations in near-global sea level pressure. *J. Atmos. Sci.*, **42**, 478–501.

Berlage, H. P., 1957: Fluctuations in the general atmospheric circulation of more than one year, their nature and prognostic value. *K. Ned. Meteor. Inst., Meded. Verh.*, **69**, 152 pp.

Bjerknes, J., 1966: A possible response of the atmospheric Hadley circulation to equatorial anomalies of ocean temperature. *Tellus*, **18**, 820–829.

——, 1969: Atmospheric teleconnections from the equatorial Pacific. *Mon. Wea. Rev.*, **97**, 163–172.

Blackmon, M. L., J. E. Geisler and E. J. Pitcher, 1983: A general circulation model study of January climate anomaly patterns associated with interannual variation of equatorial Pacific sea surface temperatures. *J. Atmos. Sci.*, **40**, 1410–1425.

Chen, W. Y., 1982: Assessment of Southern Oscillation sea level pressure indices. *Mon. Wea. Rev.*, **110**, 800–807.

Deser, C., and J. M. Wallace, 1987: El Niño events and their relationship to the Southern Oscillation: 1925–86. *J. Geophys. Res.*, **92**, 14, 189–14, 196.

Doberitz, R., 1968: Cross spectrum analysis of rainfall and sea temperature of the equatorial Pacific Ocean. *Bonner Meteor. Abhand.*, **8**, 61 pp.

Fletcher, J. O., R. J. Slutz and S. D. Woodruff, 1983: Towards a comprehensive ocean-atmosphere data set. *Trop. Ocean-Atmos. Newsletter*, **20**, 13–14.

Gordon, N. D., 1986: The Southern Oscillation and New Zealand weather. *Mon. Wea. Rev.*, **114**, 371–387.

Gutzler, D. S., and D. E. Harrison, 1987: The structure and evolution of seasonal wind anomalies over the near equatorial eastern Indian and western Pacific Oceans. *Mon. Wea. Rev.*, **115**, 169–192.

Heddinghaus, T. R., and A. F. Krueger, 1981: Annual and interannual variations in outgoing longwave radiation over the tropics. *Mon. Wea. Rev.*, **109**, 1208–1218.

Horel, J. D., and J. M. Wallace, 1981: Planetary scale atmospheric phenomena associated with the Southern Oscillation. *Mon. Wea. Rev.*, **109**, 813–829.

Jenne, R. L., 1975: *Data sets for meteorological research. Tech. Note NCAR-TN/IA-111A.* National Center for Atmospheric Research, Boulder, CO 80307, 194 pp.

Lau, N.-C., 1985: Modeling the seasonal dependence of the atmospheric response to observed El Niños in 1962–76. *Mon. Wea. Rev.*, **113**, 1970–1996.

Liebmann, B., and D. L. Hartmann, 1982: Interannual variations of outgoing IR associated with tropical circulation changes during 1974–1978. *J. Atmos. Sci.*, **39**, 1153–1162.

Meehl, G. A., 1987: The annual cycle and interannual variability in the tropical Pacific and Indian Ocean regions. *Mon. Wea. Rev.*, **115**, 27–50.

Meisner, B. N., 1976: *A study of Hawaiian and Line Island rainfall. Rep. UHMET 76-4*, Dept. Meteor., University of Hawaii, Honolulu, HI 96822, 83 pp.

Mooley, D. A., and B. Parthasarathy, 1983: Variability of the Indian summer monsoon and tropical circulation features. *Mon. Wea. Rev.*, **111**, 967–978.

Palmer, T. N., and D. A. Mansfield, 1984: Response of two atmospheric general circulation models to sea-surface temperature anomalies in the tropical East and West Pacific. *Nature*, **310**, 483–485.

——, and ——, 1986a: A study of wintertime circulation anomalies during past El Niño events using a high resolution general circulation model. I: Influence of model climatology. *Quart. J. Roy. Meteor. Soc.*, **112**, 613–638.

——, and ——, 1986b: A study of wintertime circulation anomalies during past El Niño events using a high resolution general circulation model. II: Variability of the seasonal mean response. *Quart. J. Roy. Meteor. Soc.*, **112**, 639–660.

Quinn, W. H., 1974: Monitoring and predicting El Niño invasions. *J. Appl. Meteor.*, **13**, 825–830.

——, 1979: Monitoring and predicting short-term climate changes in the South Pacific Ocean. *Proc. Int. Conf. on Mar. Sci. and Tech., Part 1*, Catholic University of Valparaiso, Valparaiso, Chile, 26–30.

Rasmusson, E. M., and T. H. Carpenter, 1982: Variations in tropical sea surface temperature and surface wind fields associated with the Southern Oscillation/El Niño. *Mon. Wea. Rev.*, **110**, 354–384.

——, and T. H. Carpenter, 1983: The relationship between eastern equatorial Pacific sea surface temperatures and rainfall over India and Sri Lanka. *Mon. Wea. Rev.*, **111**, 517–528.

——, and J. M. Wallace, 1983: Meteorological aspects of the El Niño/Southern Oscillation. *Science,* **222,** 1195–1202.

Ropelewski, C., and Halpert, M., 1987: Global and regional scale precipitation patterns associated with the El Niño/Southern Oscillation. *Mon. Wea. Rev.,* **115,** 1606–1626.

Shukla, J., and J. M. Wallace, 1983: Numerical simulation of the atmospheric response to equatorial Pacific sea surface temperature anomalies. *J. Atmos. Sci.,* **40,** 1613–1630.

Taylor, R. C., 1973: *An atlas of Pacific island rainfall. Hawaii Inst. Geophys. Data Rep. No. 25,* HIG-73-9, 175 pp. (NTIS No. AD 767073).

Trenberth, K. E., 1976a: Spatial and temporal variations of the Southern Oscillation. *Quart. J. Roy. Meteor. Soc.,* **102,** 639–653.

——, 1976b: Fluctuations in trends in indices of southern hemisphere circulation. *Quart. J. Roy. Meteor. Soc.,* **102,** 65–75.

——, 1984: Signal versus noise in the Southern Oscillation. *Mon. Wea. Rev.,* **112,** 326–332.

——, and D. Shea, 1987: On the evolution of the Southern Oscillation. *Mon. Wea. Rev.,* **115,** 3078–3096.

van Loon, H., and D. J. Shea, 1984: The Southern Oscillation. Part IV: The precursors south of 15°S to the extremes of the oscillation. *Mon. Wea. Rev.,* **112,** 947–954.

——, and ——, 1987: The Southern Oscillation. Part VI: Anomalies of sea level pressure on the Southern Hemisphere and of Pacific sea surface temperature during the development of a warm event. *Mon. Wea. Rev.,* **115,** 370–379.

Walker, G. T., and E. W. Bliss, 1932: World Weather V. *Mem. Roy. Meteor. Soc.,* **4,** 53–84.

Wright, P. B., T. P. Mitchell and J. M. Wallace, 1985: Relationships between surface observations over the global oceans and the Southern Oscillation, NOAA Data Report ERL PMEL-12, 61 pp. (available from the authors).

Wyrtki, K., 1975: El Niño—the dynamic response of the equatorial Pacific Ocean to atmospheric forcing. *J. Phys. Oceanogr.,* **5,** 572–584.